 doi:10.20944/preprints202110.0129.v1

Article

HOW ARE RED AND BLUE QUASARS DIFFERENT? THE RADIO PROPERTIES

Victoria A. Fawcett [1†*], David M. Alexander [1†], David J. Rosario [1,2†] and Lizelke Klindt [1†]

1 Centre for Extragalactic Astronomy, Department of Physics, Durham University, DH1 3LE, UK
2 School of Mathematics, Statistics and Physics, Newcastle University, NE1 7RU, UK
* Correspondence: victoria.fawcett@durham.ac.uk
† These authors contributed equally to this work.

Abstract: A non-negligible fraction of quasars are red at optical wavelengths, indicating (in the vast majority of cases) that the accretion disc is obscured by a column of dust which extinguishes the shorter-wavelength blue emission. In this paper we summarise recent work by our group, where we find fundamental differences in the radio properties of SDSS optically selected red quasars. We also present new analyses, using a consistent colour-selected quasar parent sample matched to four radio surveys (FIRST, VLA Stripe 82, VLA COSMOS 3 GHz and LoTSS DR1) across a frequency range 150 MHz-3 GHz and four orders of magnitude in radio flux. We show this enhancement is driven by systems with small-scale radio emission (∼kpc) and peaks around the radio-quiet threshold (defined as the ratio of 1.4 GHz luminosity to 6µm luminosity) across the four radio samples. Exploring the potential mechanisms behind this enhancement, we rule out star-formation and propose either small-scale jets or dusty winds interacting with the interstellar medium; this will be tested in detail using new multi-band uGMRT data. Overall our results cannot be explained with a simple viewing angle hypothesis, and so may point towards red quasars representing a key phase in the evolution of galaxies.

Keywords: Quasars; Galaxies; Radio; Supermassive Black-Holes

1. Introduction

Quasi-stellar objects (QSOs), also known as quasars, are the most powerful class of Active Galactic Nuclei (AGN). Their extremely high bolometric luminosities (up to 10^{47-48} erg s^{-1}) are now known to be caused by accretion onto a supermassive black hole (SMBH; masses of 10^8–10^9 $M_\odot$) near the Eddington limit, which places them as some of the most luminous objects in the Universe. Due to the unobscured view of the SMBH accretion disc, which peaks in the ultra-violet (UV), the majority of Type 1 QSOs have very blue optical colours. However, there is a small but significant subset with redder optical-infrared colours (referred to as "red QSOs").

Although red QSOs have been well studied in the literature, there are still conflicting views on how red and blue QSOs are related [1–12]. Some studies suggest they are intrinsically the same objects, with a red QSO simply representing a blue QSO observed at a higher inclination to the putative dusty torus, while other studies suggest an evolutionary scenario whereby a red QSO is a short-lived phase in QSO evolution. We have recently found that red QSOs show an enhancement in the radio, which cannot be explained via a simple orientation model [8–11]. The simplest result we have found is a ∼ 2–3 times higher radio detection fraction in dust-reddened Sloan Digital Sky Survey (SDSS) QSOs compared to typical blue QSOs. This radio-detection enhancement is driven by red QSOs with compact radio morphologies ($< 5''$; < 43 kpc at $z = 1.5$) and luminosities placing them around the radio-loud/radio-quiet threshold [8]. We confirmed these initial results with deeper and higher resolution data from the Very Large Array (VLA) Stripe 82, VLA COSMOS 3 GHz and LOFAR surveys [9,10]. Pushing to lower values of radio-loudness, we found that the radio enhancement decreases at extreme radio-quiet values. Analysing a sample of radio-compact red and blue QSOs with $0\farcs2$ e-MERLIN data, we found an enhancement in the nuclear–galactic scale radio emission of red QSOs [11]. Overall these

check for updates

Citation: Fawcett, V.; Alexander, D.; Rosario, D.; Klindt, L The Radio Properties of Red Quasars. *Preprints* **2021**, *1*, 0. https://doi.org/

Received:
Accepted:
Published:

Preprints (www.preprints.org) | NOT PEER-REVIEWED | Posted: 8 October 2021 doi:10.20944/preprints202110.0129.v1

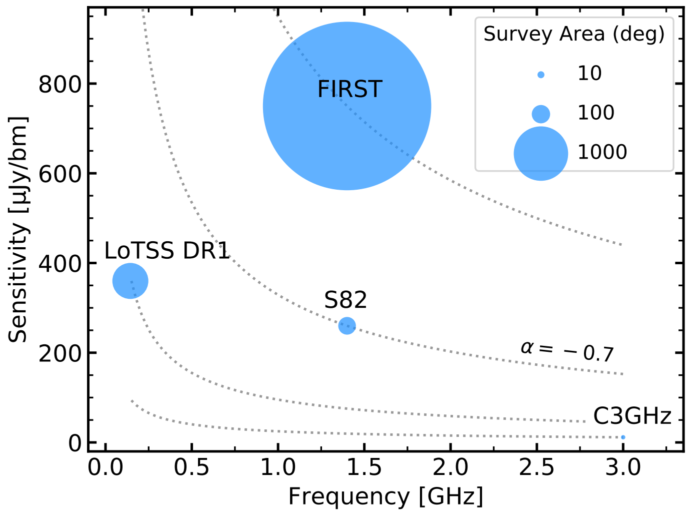

Figure 1. The 5σ sensitivity versus radio frequency for the four radio surveys considered in this paper. The survey area in degrees is indicated by the size of the marker. The dotted grey lines indicate the equivalent radio sensitivities of each of the four surveys at different frequencies for compact radio sources with $\alpha = -0.7$: for an equivalent 1.4 GHz luminosity, the S82, LoTSS DR1 and C3GHz survey sensitivities are ∼3, 10 and 38 times deeper than that of FIRST, respectively.

results are inconsistent with red QSOs being blue QSOs observed at a higher inclination angle, whereby the line of sight intersects with the top of the torus. If this were the case, we expect the opposite result; i.e., enhanced radio emission in blue QSOs due to Doppler boosting arising from a more face-on orientation of the radio jet. Therefore, there must be factors other than orientation causing this enhancement; e.g., an enhancement in small-scale jets or winds causing radio-emitting shocks in the interstellar medium (ISM).

In this paper we undertake self-consistent analyses using four different radio datasets with the same parent quasar sample to review and compare these fundamentally different radio properties of red QSOs and explore the potential mechanisms driving these differences[1]. In Section 2, we discuss the radio data and consistent QSO colour-selected samples used in this study. In Section 3.1 we use these data to explore the radio enhancement in red QSOs across four magnitudes of radio flux over radio frequencies spanning 144 MHz–3 GHz, and in Section 3.2 we compare the radio morphological sizes of red and typical QSOs. In Section 4 we discuss the potential origin of the radio emission. Throughout our work we adopt a flat Λ-cosmology with $H_0 = 70$ kms^{-1}Mpc^{-1}, $\Omega_M = 0.3$ and $\Omega_\Lambda = 0.7$.

2. Materials and Methods

In the following sections we briefly discuss the radio data used in this paper (Section 2.1: VLA FIRST, VLA Stripe 82, VLA COSMOS 3 GHz and LoTSS DR1; for full details, refer to the references within each subsection), the optical data used to construct our QSO parent sample (Section 2.2) and our final colour- and radio-detected samples (Section 2.3).

2.1. Radio Data

An illustration of the sensitivity, frequency and sky coverage for each radio survey used in this paper is shown in Fig. 1. This highlights how some radio surveys have impressive source statistics, but are lacking in sensitivity (e.g. FIRST), whereas others are extremely sensitive, but only cover a very small area of the sky (e.g. C3GHz).

[1] Our previous studies had small differences in the selection of the QSO samples: e.g. different SDSS data releases and different sized control samples.

Preprints (www.preprints.org) | NOT PEER-REVIEWED | Posted: 8 October 2021 doi:10.20944/preprints202110.0129.v1

2.1.1. VLA FIRST

The Faint Images of the Radio Sky (FIRST) radio survey covers 9055 deg^2 of the North Galactic Cap and Equatorial Strip in the SDSS region. FIRST has a 5$''$ resolution at 1.4 GHz taken primarily in the VLA B-configuration. The catalogue contains 946 000 sources with a typical sensitivity of 0.15 mJy/bm; 30% of the FIRST sources have optical counterparts in the SDSS [13].

2.1.2. VLA Stripe 82 (S82)

Stripe 82 is a $\sim$300 deg^2 equatorial field that has been imaged multiple times by SDSS [14]. It spans a right ascension of $\alpha = -50°$ to $+59°$ and a declination of $\delta = -1.25°$ to $1.25°$. The 1.4 GHz high-resolution radio survey (S82; [15]), covers $\sim$92 deg^2 and has a $1''.8$ spatial resolution, taken primarily in the A-configuration. At its median sensitivity of 52 μJy/bm, S82 is roughly three times deeper than that of FIRST.

In the catalogue provided in [15], peak flux densities ($F_{\rm peak}$) are derived by fitting an elliptical Gaussian model to the source. Matching to the FIRST catalogue recovers over 97% of the FIRST-detected QSOs in this region [15].

2.1.3. VLA-COSMOS 3 GHz (C3GHz)

The VLA-COSMOS 3 GHz (C3GHz) survey spans 2.6 deg^2 at 3 GHz, centred on the COSMOS field (RA = 10:00:28.6, Dec = +02:12:21.0) at a $0''.75$ spatial resolution in the A+C configuration [16]. At its median sensitivity of $\sim$2.3 μJy/bm, C3GHz is equivalently $\sim$ 13 times deeper than the S82 and $\sim$ 38 times deeper than FIRST at 1.4 GHz, assuming a spectral index of $\alpha = -0.7$ ($S_\nu \propto \nu^\alpha$). In the catalogue provided in [16], $F_{\rm peak}$ is measured by fitting a two-dimensional parabola around the brightest pixel. On the basis of a Monte Carlo method, the source completeness is 55% up to 20 μJy, which rises to 94% above 40 μJy.

The COSMOS field has also been observed at 1.4 GHz over 2 deg^2 in an earlier VLA radio survey [17]. This survey has a resolution of $1''.5 \times 1''.4$ and a sensitivity of $\sim$10.5 μJy/bm ($\sim$5 times deeper than S82). To calculate the $L_{1.4\,\rm GHz}$, the 1.4 GHz flux from this survey ([17]) is used, when available, and scaled from the 3 GHz flux using a spectral index of -0.7, otherwise.

2.1.4. LoTSS DR1

The LOFAR Two-metre Sky Survey (LoTSS) is a 120–168 MHz survey of northern sky at a resolution of 6″ [18]. The first full-resolution data release (DR1; [19]) covers 424 deg^2 in the HETDEX spring field (RA = 10h45m to 15h30m, Dec = 45° to 47°). At it's median sensitivity of 71 μJy/bm, LoTSS is equivalently $\sim$ 3.5 times deeper than S82 and $\sim$ 10 times deeper than FIRST at 1.4 GHz, assuming a spectral index of $\alpha = -0.7$. To calculate the $L_{1.4\,\rm GHz}$, the 144 MHz fluxes are scaled to 1.4 GHz using a spectral index of -0.7.

2.2. *Optical data: the SDSS DR14 Quasar Catalogue*

The SDSS DR14 Quasar Catalogue contains 526 356 spectroscopically selected QSOs across a 9376 deg^2 region, out to redshifts around $z = 7$ [20]. The catalogue includes previous spectroscopically-confirmed QSOs from the SDSS-I and II Legacy surveys [21] with QSOs targeted by the Baryon Oscillation Spectroscopic Survey (BOSS; [22]) in SDSS-III [23] and the extended Baryon Oscillation Spectroscopic Survey (eBOSS; [24]) in SDSS-IV.

In this paper, the SDSS five-band optical photometry ($u^*g^*r^*i^*z^*$) is also utilised, corrected by the associated band-dependent Galactic extinction estimates. The quasar catalogue provides spectroscopic redshifts based on different estimators [20]; in this work we use the most robust of these estimates (listed as Z in the catalogue).

2.3. *Colour-selected and radio-detected samples*

To define our sample of colour-selected QSOs we used the g^* (4770 Å) and i^* (7625 Å) band extinction-corrected photometry in the DR14 catalogue and followed a similar approach to our previous studies [8–10]. First we restricted to a redshift range of $0.2 < z < 2.4$

Preprints (www.preprints.org) | NOT PEER-REVIEWED | Posted: 8 October 2021 doi:10.20944/preprints202110.0129.v1

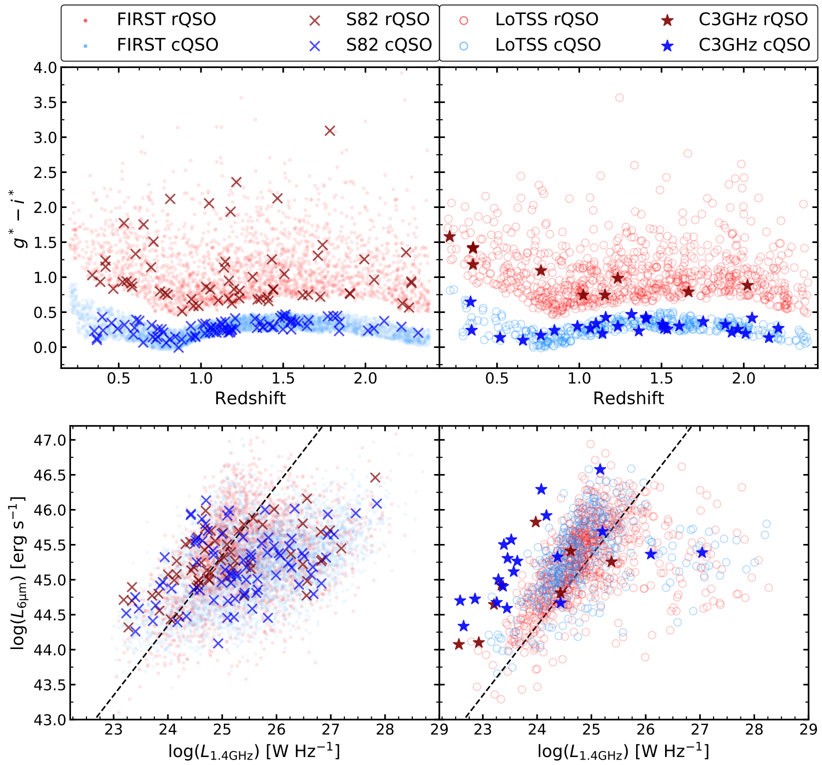

Figure 2. $g^* - i^*$ versus redshift (top panel) and $L_{6\mu\mathrm{m}}$ versus $L_{1.4\,\mathrm{GHz}}$ (bottom panel) of the radio-detected FIRST (dots), S82 (crosses), LoTSS (circles) and C3GHz (stars), rQSOs (red) and cQSOs (blue). It is worth noting that the rQSO and cQSO thresholds were calculated using the full parent QSO sample. Our division between radio-loud and radio-quiet sources ($\mathcal{R} = -4.2$) is displayed as a dashed line in the bottom panel. To calculate the equivalent 1.4 GHz luminosity for the LoTSS and C3GHz samples, we assume a spectral index of $\alpha = -0.7$ (see Fig. 1).

to ensure our colour selection is not affected by the Lyman break and that we are excluding lower luminosity sources. In order to control for the impact of redshift on the $g^* - i^*$ colour selections, we sorted the QSOs by redshift and constructed $g^* - i^*$ distributions in contiguous bins of 1000 sources. Our red and control QSOs (hereafter, rQSOs and cQSOs) were then selected above the top 90th percentile and within the middle 50th percentile of the observed SDSS $g^* - i^*$ distribution, respectively; the cQSOs therefore represent typical QSOs in terms of their colour.

Due to the loss of flux at UV-optical wavelengths, dust-reddened optically-selected rQSOs will be biased towards higher luminosities compared to typical QSOs at similar redshifts. Therefore, in order to ensure that our results are not due to differences in the intrinsic luminosity distributions of rQSOs and cQSOs, we also matched the samples in both redshift and luminosity: for this, we use the rest-frame 6µm luminosity ($L_{6\mu\mathrm{m}}$) since this provides an extinction-insensitive measure of the intrinsic luminosity (e.g. [25–28]). To calculate $L_{6\mu\mathrm{m}}$ we identified mid-infrared (MIR) counterparts from the the Wide-Field Infrared Survey Explorer (*WISE*; [29]), an all-sky survey which provides photometry in four bands (3.4, 4.6, 12 and 22 µm). We used the NASA/IPAC query engine to match the SDSS DR14 QSOs to the All-Sky *WISE* Source Catalogue (ALL-*WISE*) adopting a 2.″7 search radius, which ensures a 95.5% positional certainty [30], and required a detection with a signal-to-noise ratio (SNR) of greater than 2 in the *WISE W1*, *W2* and *W3* bands in order to derive an accurate estimate of their $L_{6\mu\mathrm{m}}$. For the final colour-selected samples, we match

Preprints (www.preprints.org) | NOT PEER-REVIEWED | Posted: 8 October 2021 doi:10.20944/preprints202110.0129.v1

Sample	ν [GHz]	Area [deg^2]	Colour-selected rQSOs	Colour-selected cQSOs	Radio-detected rQSOs	Radio-detected cQSOs	Radio enhance.
FIRST	1.4	10 000	20 546	20 546	2339 (11.4%)	940 (4.6%)	2.5
S82	1.4	92	372	1668	61 (16.4%)	82 (4.9%)	3.3
C3GHz	3	2.6	10	29	8 (80.0%)	20 (69.0%)	1.2
LoTSS	0.15	424	2223	1822	802 (36.1%)	368 (20.2%)	1.8

Table 1: The columns from left to right display the: (1) radio frequency of each dataset, (2) radio survey area, (3) number of rQSOs and cQSOs in the parent samples within each radio survey region, (4) the number of radio-detected rQSOs and cQSOs (the radio-detection fractions for each colour-selected sample is displayed in the brackets), and (5) the radio enhancement of rQSOs over cQSOs; the radio enhancement for the rQSOs is > 1 in each sample. It should be noted that the samples in italics are not matched in $L_{6\mu m}$ due to lack of sources.

in $L_{6\mu m}$ and redshift, using a tolerance of 0.2 and 0.05 dex, respectively[2], following a similar approach to [8] (see Section 2.3.2 therein).

For our study here, the colour-selected QSO sample was then restricted to the various radio survey regions, using non-zero local root mean square (RMS) values either provided through a radio mosaic or an online matching server. The resulting number of colour-selected and radio-detected rQSOs and cQSOs for each of the four radio surveys explored in this work are displayed in Table 1; the radio-detection fraction and enhancement[3] in the rQSOs compared to the cQSOs are also shown. To quantify how many of the rQSOs and cQSOs in our sample are 'radio-quiet' we adopted the same "radio-loudness" parameter ($\mathcal{R}$) as that first used in [8], defined as the dimensionless quantity:

$$\mathcal{R} = \log_{10} \frac{L_{1.4\,\mathrm{GHz}}}{L_{6\mu\mathrm{m}}}. \quad (1)$$

We also used the same radio-loud/radio-quiet threshold of $\mathcal{R} = -4.2$, equivalent to a mechanical-to-radiative power ratio of $P_{\mathrm{mech,sync}}/P_{\mathrm{rad},L_{6\mu m}} \approx 0.001$, which is broadly consistent with the classical radio-quiet/radio-loud threshold often defined using a 5 GHz-to-2500 Å flux ratio, but is less susceptible to obscuration from dust (see [8] for full details).

The $g^* - i^*$ colour versus redshift and $L_{6\mu m}$ versus $L_{1.4\,\mathrm{GHz}}$ distributions for the four radio-detected colour-selected samples explored in this paper, are shown in the top and bottom panels of Fig. 2, respectively. The $g^* - i^*$ distribution shows that, despite encompassing 50% of the parent QSO population, the cQSOs cover a narrow region of colour space, compared to the broad swathe of colour space encompassed by the top 10% rQSOs.

3. Results

In this section we use the same colour-selected QSO sample, matched in both redshift and 6µm luminosity, in order to apply self-consistent analyses of the radio properties of rQSOs, using radio data from four different radio surveys, spanning radio frequencies of 0.144–3 GHz and equivalent 1.4 GHz radio fluxes of ∼0.01–1000 mJy.

3.1. Radio enhancement in rQSOs

In the bottom panel of Fig. 2 we show the $L_{6\mu m}$ versus $L_{1.4\,\mathrm{GHz}}$ distributions for the four radio-detected samples used in our analyses. The differences in the distributions of the data in Fig. 2 is related to the depth and areal coverage of the radio surveys. The C3GHz has the most sensitive radio data, probing down to very low $\mathcal{R}$ values, but covers a small area and consequently few luminous radio-sources are detected. By comparison,

[2] Due to a lack of sources, we are unable to match in luminosity for the S82 or C3GHz samples.
[3] Defined as the radio-detection fraction of the rQSOs, divided by the radio-detection fraction of the cQSOs.

 doi:10.20944/preprints202110.0129.v1

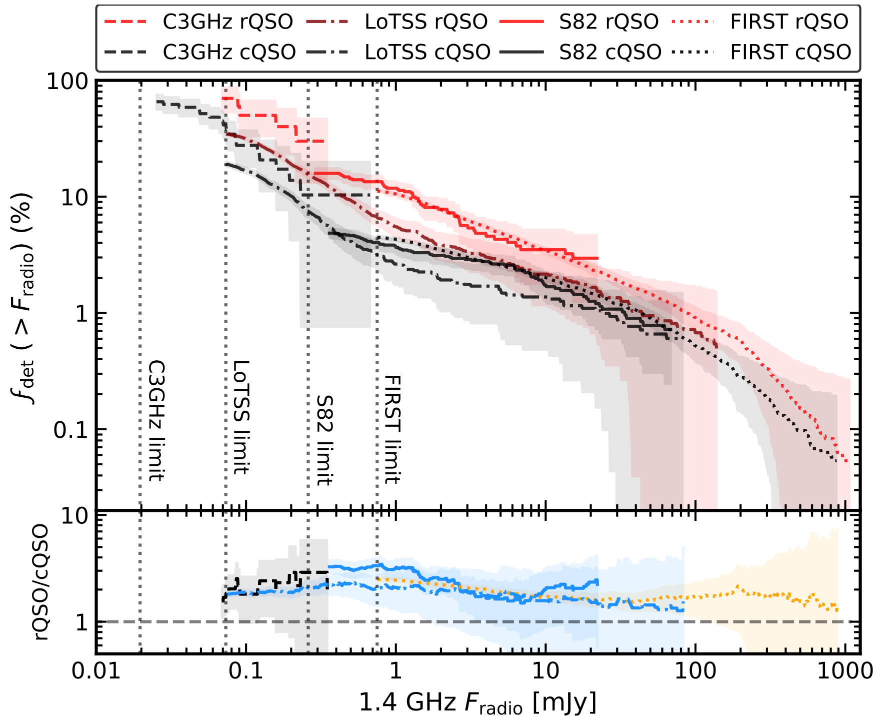

Figure 3. Cumulative radio-detection fraction as a function of 1.4 GHz flux for the four rQSO and cQSO radio-detected samples. The bottom panel displays the 2–3 times radio enhancement of the rQSOs; across 4 orders of magnitude a larger fraction of rQSOs are radio detected than compared to cQSOs. The shaded error region was calculated using the method described in [31] and corresponds to 1σ binomial uncertainties.

the other surveys cover large areas and detect QSOs across a broad range of the $\mathcal{R}$ plane, providing good coverage overall particularly from the sensitive LoTSS survey. Fig. 3 displays the cumulative radio-detection fraction of our four samples as a function of the 1.4 GHz radio flux. Across four orders of magnitude in 1.4 GHz flux, the rQSOs have a 2–3 higher radio-detection fraction in all four radio samples.

Splitting the radio-detected samples into contiguous $\mathcal{R}$ bins, we calculated the enhancement in the radio-detection fraction of the full colour-selected sample for the rQSOs. This is calculated as the ratio of the radio-detection fraction of the rQSOs to the radio-detection fraction of the cQSOs in each sample (see our previous studies for more details [8–10]). Fig. 4 displays the radio enhancement for the FIRST (shaded orange), combined S82+C3GHz (shaded blue) and LoTSS- (shaded grey) detected samples. All three of these samples peak around $\mathcal{R} \sim -4.5$ with a factor ∼3–6 excess in the red QSOs, decreasing to around unity towards the extreme radio-loud and radio-quiet values, as found in our previous work [9,10]. We will explore this decrease in Section 4.1.

3.2. Radio morphology

The majority of the radio-detected rQSOs that contribute to the radio-excess shown in Fig. 4 have compact morphologies at the resolution of FIRST (5″; ∼ 43 kpc at $z = 1.5$ [8]). However, these size constraints are just upper limits, and higher-resolution radio data has shown that the rQSOs are typically compact over galaxy scales (e.g., < 16 kpc on the basis of 1.″8 resolution data in the S82 field [9]).

Most recently we have obtained 0.″2 e-MERLIN radio data for19 and 20 FIRST radio-compact rQSOs and cQSOs, finding that the majority remain unresolved (suggesting < 2 kpc scales) but also revealing a tentative enhancement in the fraction of rQSOs that are resolved over the ∼ 2–10 kpc scales of the host galaxy [11]. A comparison of the radio image of two rQSOs at FIRST 5″ resolution and e-MERLIN 0.″2 resolution is shown in

 doi:10.20944/preprints202110.0129.v1

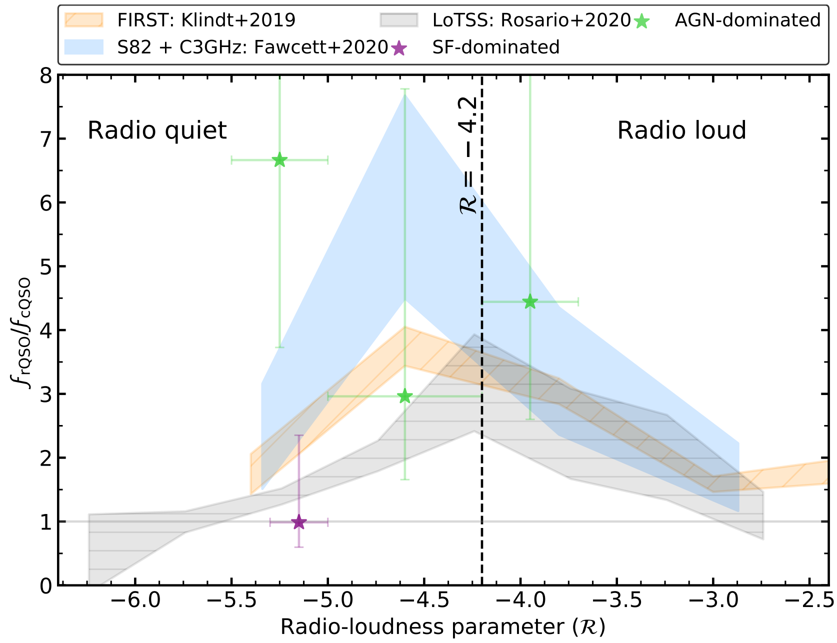

Figure 4. Radio-detection enhancement as a function of radio-loudness for the FIRST (orange), LoTSS (grey), and combined S82 and C3GHz (blue) samples. Our defined radio-quiet threshold ($\mathcal{R} = -4.2$) is displayed as a dashed vertical line. The radio enhancement of the C3GHz rQSOs with radio emission dominated by SF is shown as a purple star, and those with radio emission dominated by AGN processes is shown as green stars.

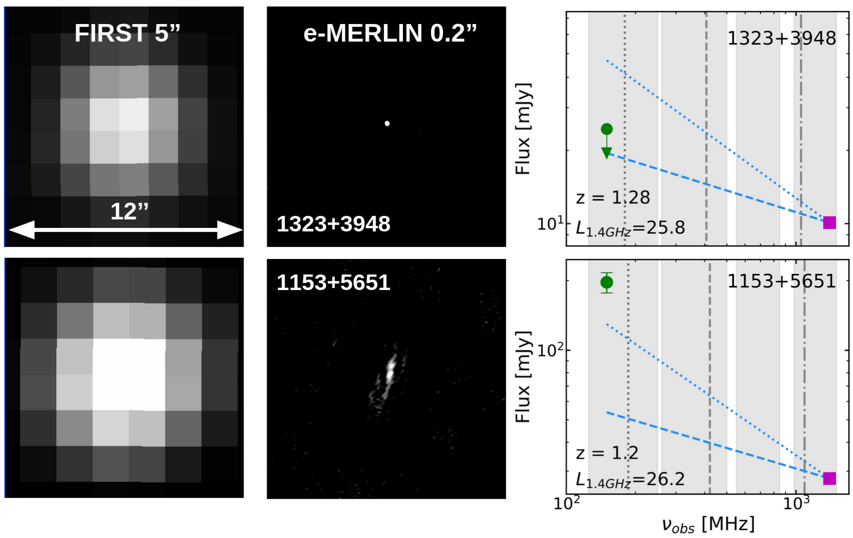

Figure 5. $12'' \times 12''$ thumbnails of two rQSOs unresolved at FIRST 5″ resolution (left), observed in the e-MERLIN 0.″2 data (middle) from [11]; the top source remains unresolved at the e-MERLIN resolution but the bottom source shows ∼kpc-scale extended radio emission. (Right) radio flux vs frequency for the two sources displayed in the thumbnails, using 150 MHz data from TGSS and 1.4 GHz data from FIRST; a 7σ upper limit of 24.5 µJy is used for the TGSS-undetected source (top). The grey shaded regions demonstrate the four radio bands over which we have recently obtained uGMRT data for all of our e-MERLIN observed sources, allowing us to construct sensitive radio SEDs (PI: V. Fawcett). The dashed and dotted blue lines indicate the expected fluxes for a spectral slope of $\alpha = -0.3$ and $\alpha = -0.7$, respectively, demonstrating the variety in radio spectral slopes within the FIRST-compact sources. The vertical lines show the frequencies expected for GPS/CSS-like sources of 0.1, 0.5 and 2 kpc extents. This demonstrates that for the unresolved e-MERLIN source, with the uGMRT data we will be able to constrain the radio sizes to < 1 kpc scale, below the resolution of the e-MERLIN data.

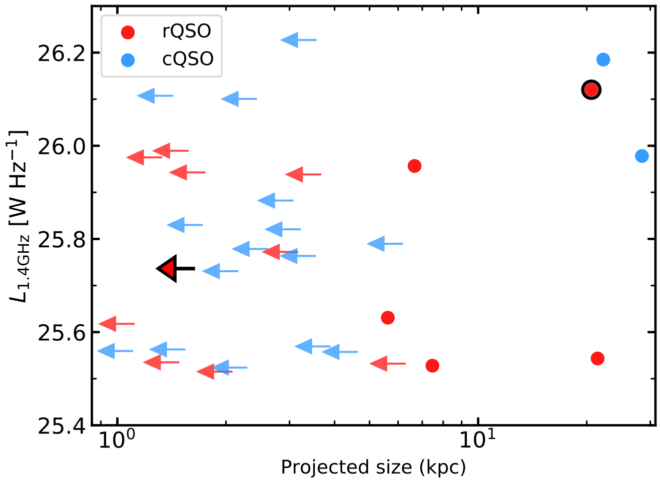

Figure 6. $L_{1.4\,\mathrm{GHz}}$ vs projected size for the e-MERLIN rQSOs and cQSOs from [11]. The resolved sources are displayed as circles and the unresolved sources are shown as upper limits. The two rQSOs displayed in Fig. 5 are outlined in black: source 1153+5651 is resolved and 1323+3948 is unresolved.

the left of Fig. 5: in the lower example, there is clear extended emission at e-MERLIN resolutions, while the upper example remains unresolved. Fig. 6 displays the $L_{1.4\,\mathrm{GHz}}$ vs projected size of the e-MERLIN rQSOs and cQSOs: resolved sources are shown as circles and unresolved sources are shown as upper limits. The resolved and unresolved source displayed in the thumbnails of Fig. 5 are outlined in black. Radio data sensitive to smaller spatial scales (e.g., VLBA observations at $\sim 0.''01$) is required to directly measure the size scale for the majority of the sources that contribute to the radio excess.

4. Discussion

In this paper we have reviewed our recent research that identified fundamental differences in the radio properties between rQSOs and cQSOs. We also undertook a series of new analyses using the same colour-selected QSO sample, which we then matched to four different radio surveys at various depths and frequencies. This allowed us to perform self-consistent analyses based on the same QSO sample across the different radio datasets. We confirmed our previous radio results, finding an enhancement in the radio-detection fraction of rQSOs compared to cQSOs that arises in radio compact systems around the radio-quiet threshold [8–11]. This small-scale enhanced radio emission found in red QSOs could be driven by star-formation or AGN processes: in the following sections we discuss these different scenarios.

4.1. Origin of the radio emission: star-formation

In order to assess whether the radio-quiet emission in rQSOs is dominated by SF, in a previous study we utilised the multi-wavelength data available in the COSMOS field [9]. Using the rest-frame (8–1000 μm) IR luminosity constraints on SF preferentially from [32], and from [33] when not available, we defined the origin of the radio emission as dominated by SF if the measured radio luminosity is within a factor of 3 of the radio-FIR relationship for star-forming galaxies. Otherwise, the source is defined as AGN-dominated. Using this, we then split the lower radio-loudness bins covered by our C3GHz sample, into sources with radio emission either dominated by SF or AGN (purple and green stars, respectively; see Fig. 4). From this it is clear that for an $\mathcal{R} < -5$, SF-dominated sources have a radio enhancement consistent with unity (albeit low source statistics). We also found the AGN-dominated sources, although very uncertain, are consistent with being enhanced at all values of $\mathcal{R}$, suggesting that the radio enhancement in rQSOs is driven by AGN mechanisms. In a separate spectral energy distribution (SED) analysis of a sample of

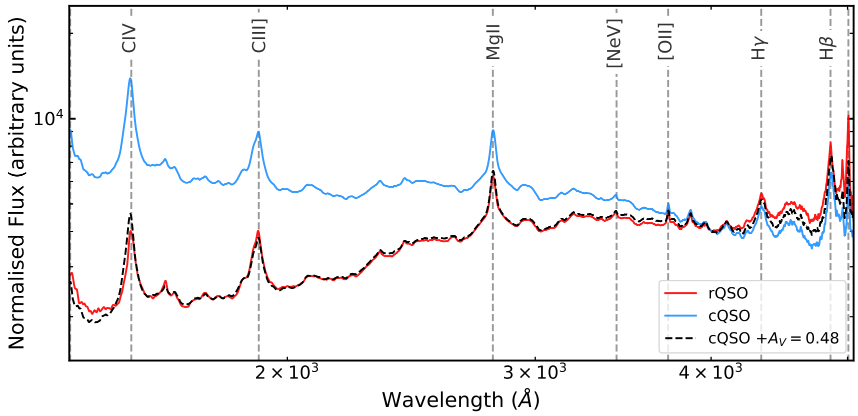

Figure 7. SDSS DR14 composites for our rQSO (red) and cQSO (blue) samples, in a redshift range $1.0 < z < 1.6$ and luminosity range $45.3 < \log L_{6\mu m} < 47.0\,\mathrm{erg\,s^{-1}}$. The dotted black line shows the cQSO composite with a dust extinction of $A_V = 0.5$ mags that is remarkably similar to the rQSO composite. This amount of dust extinction is consistent with that found from fitting the individual VLT X-shooter spectra of a sample of rQSOs and cQSOs at $z \sim 1.5$ (Fawcett et al. *in prep*) and in our SED analysis of SDSS rQSOs and cQSOs [12]. The major emission lines are indicated by a dashed vertical grey line.

rQSOs and cQSOs, we found no differences in the SF properties [12]; this provides indirect evidence that the radio enhancement is due to AGN activity.

4.2. Origin of the radio emission: AGN

The small spatial scales for the radio emission from the majority of the e-MERLIN observed sources suggests the radio enhancement in rQSOs occurs at $< 2\,$kpc. These projected size scales are consistent with those typical of Compact Steep Spectrum (CSS) sources and Gigahertz-Peaked Spectrum (GPS); these are known to be jet-dominated radio sources. Our future work analysing 4-band 150 MHz–1.4 GHz upgraded Giant Metre Radio Telescope (uGMRT) data of this same sample (PI: V. Fawcett) will be crucial for determining the spectral turnover (or lack thereof) of rQSOs and cQSOs in order to test this CSS/GPS hypothesis. The right plot of Fig. 5 displays the radio SEDs of the two sources shown in the left thumbnails, using data from the 150 MHz all sky TGSS survey [34] (or an upper limit for the undetected unresolved source) and FIRST. The dashed and dotted blue lines indicate the expected fluxes for a spectral slope of $\alpha = -0.3$ and $\alpha = -0.7$, respectively. The vertical lines show the frequencies expected for GPS/CSS-like sources of 0.1, 0.5 and 2 kpc extents [35]. The radio SED for the unresolved source demonstrates that with the uGMRT data we will be able to constrain the radio sizes to $< 1\,$kpc scales: this could suggest the presence of a compact jet.

However, if the enhanced radio emission is due to small-scale jets then it is not immediately clear why there would be a close connection between the radio emission and optical colour. Exploring the origin of the red colours, in Fawcett et al. (*in prep*) we use broad-wavelength Very Large Telescope (VLT) X-shooter [36] spectra to explore the cause of the red colours and find that the reddening in rQSOs is fully consistent with being caused by moderate amounts of dust ($A_V \sim 0.1$–1 mags), also found in our previous work [12]. To further demonstrate this, Fig. 7 displays DR14 SDSS rQSO (red) and cQSO (blue) median composites, in a redshift range $1.0 < z < 1.6$ and luminosity range $45.3 < \log L_{6\mu m} < 47.0\,\mathrm{erg\,s^{-1}}$. A dust-reddened cQSO composite ($A_V \sim 0.5$ mags) is shown by the dotted black line, which describes the shape of the red composite remarkably well. A direct connection between the presence of dust and radio emission could be through shocks, whereby a dusty wind from the nucleus interacts with the ISM. We have previously found evidence for larger FWHMs in the broader wing component of the [O III]λ5007 in rQSOs compared to cQSOs at $z < 0.8$; evidence for stronger winds within the rQSO population. In Alexander et al. (*in prep*), we also find a link between rQSOs and Low-ionization Broad Absorption Line Quasars (LoBALs; BALQSOs that display additional low-ionization species such as Mg II and Al III, e.g. [37]); LoBALs tend to have redder optical colours on average and display similar radio properties to rQSOs (also identified in other studies, e.g. [38]). However, the fact we also find a radio enhancement in red nonBALs suggests that outflow power is not strongly connected to the radio emission; the radio enhancement in rQSOs may be more closely related to the dust opacity of the wind. Therefore, although we cannot rule out small-scale jets, wind-driven shocks in the ISM can more directly associate the excess radio with the presence of dust.

5. Conclusions

We have reviewed our recent research that identified fundamental differences in the radio properties between a sample of $0.2 < z < 2.4$ red and typical QSOs. We have also undertaken new, self-consistent analyses using the same DR14 QSO parent sample, confirming previous results but for the first time utilising four different radio datasets at various frequencies and depths: FIRST, S82, C3GHz and LoTSS DR1. Overall we find:

- **Enhanced radio emission in red QSOs that peaks around the radio-quiet threshold (see Fig. 3 and 4):** We find an enhancement in the radio-detection fraction of red QSOs across a 1.4 GHz radio flux range of 0.1–1000 mJy. Exploring the radio-loudness parameter, we show that the radio enhancement in all four samples peaks around the radio-quiet threshold and decreases towards both the extreme radio-loud and radio-quiet ends.
- **Red QSOs show tentative differences in galaxy-scale radio emission (see Fig. 5 and 6):** Probing the ∼kpc scales with e-MERLIN we have showed that the majority of FIRST radio compact systems remain unresolved. The high-resolution e-MERLIN data also reveals an enhancement in the slightly extended, galaxy-scale radio emission of red QSOs when compared to blue QSOs. Radio data sensitive to emission on smaller scales is required to resolve the scales of the unresolved sources (e.g. VLBA, uGMRT).
- **The enhanced radio emission is likely due to AGN processes (see Section 4):** Using FIR data in the COSMOS field, we showed that the radio emission is driven by AGN processes (see Fig. 4) which is consistent with our previous work [12]. We cannot rule out small-scale jets as the origin of the radio emission but argue that wind-driven shocks can more directly associate the excess radio with the presence of dust; e.g., in the ISM/circumnuclear environment.

We summarise results on the fundamentally different radio properties of red QSOs when compared to typical blue QSOs. Emerging evidence suggests that the link between these radio properties and the redness of a QSO may be related to a wind and opacity/dust associated with the nucleus or ISM in the host galaxy; therefore red QSOs may be an important population to study within the context of quasar evolution. Our future uGMRT study will further investigate small-scale jets versus dusty winds as the origin of the radio emission. Using the Dark Energy Spectroscopic Instrument (DESI; [39]), we will push to fainter and more heavily obscured QSOs in order to test whether the radio properties we find in SDSS QSOs extend to more extreme systems.

Author Contributions: All authors contributed equally to this manuscript subject to the following sections: data curation, V. A. Fawcett; original draft preparation, V. A. Fawcett; supervision, D. M. Alexander and D.J. Rosario; project administration, D. M. Alexander and D.J. Rosario. All authors have read and agreed to the published version of the manuscript.

Funding: We acknowledge a quota studentship through grant code ST/S505365/1 funded by the Science and Technology Facility Council (VAF), the Faculty of Science Durham Doctoral Scholarship (LK), the Science and Technology Facilities Council (DMA, DJR, through grant codes ST/P000541/1 and ST/T000244/1).

Funding for the Sloan Digital Sky Survey has been provided by the Alfred P. Sloan Foundation, the U.S. Department of Energy Office of Science, and the Participating Institutions. SDSS-IV acknowledges support and resources from the Center for High-Performance Computing at the University of Utah.

Institutional Review Board Statement: Not applicable.

Acknowledgments: The SDSS web site is www.sdss.org. SDSS-IV, the primary data set used in this analysis, is managed by the Astrophysical Research Consortium for the Participating Institutions of the SDSS Collaboration including the Brazilian Participation Group, the Carnegie Institution for Science, Carnegie Mellon University, the Chilean Participation Group, the French Participation Group, Harvard-Smithsonian Center for Astrophysics, Instituto de Astrofísica de Canarias, The Johns Hopkins University, Kavli Institute for the Physics and Mathematics of the Universe (IPMU) / University of Tokyo, the Korean Participation Group, Lawrence Berkeley National Laboratory, Leibniz Institut für Astrophysik Potsdam (AIP), Max-Planck-Institut für Astronomie (MPIA Heidelberg), Max-Planck-Institut für Astrophysik (MPA Garching), Max-Planck-Institut für Extraterrestrische Physik (MPE), National Astronomical Observatories of China, New Mexico State University, New York University, University of Notre Dame, Observatário Nacional / MCTI, The Ohio State University, Pennsylvania State University, Shanghai Astronomical Observatory, United Kingdom Participation Group, Universidad Nacional Autónoma de México, University of Arizona, University of Colorado Boulder, University of Oxford, University of Portsmouth, University of Utah, University of Virginia, University of Washington, University of Wisconsin, Vanderbilt University, and Yale University.

This publication makes use of data products from the Wide-field Infrared Survey Explorer, which is a joint project of the University of California, Los Angeles, and the Jet Propulsion Laboratory/California Institute of Technology, funded by the National Aeronautics and Space Administration.

The National Radio Astronomy Observatory is a facility of the National Science Foundation operated under cooperative agreement by Associated Universities, Inc.

Conflicts of Interest: The authors declare no conflict of interest. The funders had no role in the design of the study; in the collection, analyses, or interpretation of data; in the writing of the manuscript, or in the decision to publish the results.

Abbreviations

The following abbreviations are used in this manuscript:

AGN	Active Galactic Nuclei
BALQSO	Broad Absorption Line Quasar
COSMOS	The Cosmic Evolution Survey
cQSO	Control Quasar
CSS	Compact Steep Spectrum
C3GHZ	COSMOS 3 GHz
e-MERLIN	Extended Multi-Element Radio-Linked Interferometer Network
FIRST	Faint Images of the Radio Sky at Twenty-cm
GPS	Gigahertz-Peaked Spectrum
LoBAL	Low-ionization Broad Absorption Line quasar
LOFAR	LOw Frequency ARray
LoTSS	The LOFAR Two-metre Sky Survey
QSO	Quasi-stellar object
rQSO	Red Quasar
RMS	Root Mean Square
SDSS	Sloan Digital Sky Survey
SED	spectral energy distribution
SF	star-formation
S82	Stripe 82
TGSS	TIFR GMRT Sky Survey
uGMRT	upgraded Giant Metrewave Radio Telescope
VLA	Very Large Array
VLT	Very Large Telescope
WISE	Wide-Field Infrared Survey Explorer

References

1. Richards, G.T.; Hall, P.B.; Vand en Berk, D.E.; Strauss, M.A.; Schneider, D.P.; Weinstein, M.A.; Reichard, T.A.; York, D.G.; Knapp, G.R.; Fan, X.; Ivezić, Ž.; Brinkmann, J.; Budavári, T.; Csabai, I.; Nichol, R.C. Red and Reddened Quasars in the Sloan Digital Sky Survey. *AJ* **2003**, *126*, 1131–1147, [arXiv:astro-ph/astro-ph/0305305]. doi:10.1086/377014.
2. Glikman, E.; Helfand, D.J.; White, R.L.; Becker, R.H.; Gregg, M.D.; Lacy, M. The FIRST-2MASS Red Quasar Survey. *ApJ* **2007**, *667*, 673–703, [arXiv:astro-ph/0706.3222]. doi:10.1086/521073.
3. Georgakakis, A.; Clements, D.L.; Bendo, G.; Rowan-Robinson, M.; Nandra, K.; Brotherton, M.S. Are red 2MASS QSOs young? *MNRAS* **2009**, *394*, 533–546, [http://oup.prod.sis.lan/mnras/article-pdf/394/1/533/3882498/mnras0394-0533.pdf]. doi:10.1111/j.1365-2966.2008.14344.x.
4. Urrutia, T.; Becker, R.H.; White, R.L.; Glikman, E.; Lacy, M.; Hodge, J.; Gregg, M.D. THE FIRST-2MASS RED QUASAR SURVEY. II. AN ANOMALOUSLY HIGH FRACTION OF LoBALs IN SEARCHES FOR DUST-REDDENED QUASARS. *ApJ* **2009**, *698*, 1095–1109. doi:10.1088/0004-637x/698/2/1095.
5. Banerji, M.; McMahon, R.G.; Hewett, P.C.; Alaghband-Zadeh, S.; Gonzalez-Solares, E.; Venemans, B.P.; Hawthorn, M.J. Heavily reddened quasars at $z \sim 2$ in the UKIDSS Large Area Survey: a transitional phase in AGN evolution. *MNRAS* **2012**, *427*, 2275–2291, [arXiv:astro-ph.CO/1203.5530]. doi:10.1111/j.1365-2966.2012.22099.x.
6. Glikman, E.; Urrutia, T.; Lacy, M.; Djorgovski, S.G.; Mahabal, A.; Myers, A.D.; Ross, N.P.; Petitjean, P.; Ge, J.; Schneider, D.P.; York, D.G. FIRST-2MASS Red Quasars: Transitional Objects Emerging from the Dust. *ApJ* **2012**, *757*, 51, [1207.2175]. doi:10.1088/0004-637X/757/1/51.
7. Kim, D.; Im, M. What makes red quasars red?. Observational evidence for dust extinction from line ratio analysis. *A&A* **2018**, *610*, A31, [arXiv:astro-ph.GA/1712.01851]. doi:10.1051/0004-6361/201731963.
8. Klindt, L.; Alexander, D.M.; Rosario, D.J.; Lusso, E.; Fotopoulou, S. Fundamental differences in the radio properties of red and blue quasars: evolution strongly favoured over orientation. *MNRAS* **2019**, *488*, 3109–3128, [arXiv:astro-ph.GA/1905.12108]. doi:10.1093/mnras/stz1771.
9. Fawcett, V.A.; Alexander, D.M.; Rosario, D.J.; Klindt, L.; Fotopoulou, S.; Lusso, E.; Morabito, L.K.; Calistro Rivera, G. Fundamental differences in the radio properties of red and blue quasars: enhanced compact AGN emission in red quasars. *MNRAS* **2020**, *494*, 4802–4818, [arXiv:astro-ph.GA/2004.01197]. doi:10.1093/mnras/staa954.
10. Rosario, D.J.; Fawcett, V.A.; Klindt, L.; Alexander, D.M.; Morabito, L.K.; Fotopoulou, S.; Lusso, E.; Calistro Rivera, G. Fundamental differences in the radio properties of red and blue quasars: insight from the LOFAR Two-metre Sky Survey (LoTSS). *MNRAS* **2020**, *494*, 3061–3079, [arXiv:astro-ph.GA/2004.01196]. doi:10.1093/mnras/staa866.
11. Rosario, D.J.; Alexander, D.M.; Moldon, J.; Klindt, L.; Thomson, A.P.; Morabito, L.; Fawcett, V.A.; Harrison, C.M. Fundamental differences in the radio properties of red and blue quasars: kiloparsec-scale structures revealed by e-MERLIN. *MNRAS* **2021**, *505*, 5283–5300, [arXiv:astro-ph.GA/2106.02646]. doi:10.1093/mnras/stab1653.
12. Calistro Rivera, G.; Alexander, D.M.; Rosario, D.J.; Harrison, C.M.; Stalevski, M.; Rakshit, S.; Fawcett, V.A.; Morabito, L.K.; Klindt, L.; Best, P.N.; Bonato, M.; Bowler, R.A.A.; Costa, T.; Kondapally, R. The multiwavelength properties of red QSOs: Evidence for dusty winds as the origin of QSO reddening. *A&A* **2021**, *649*, A102, [arXiv:astro-ph.GA/2103.02610]. doi:10.1051/0004-6361/202040214.
13. Becker, R.H.; White, R.L.; Helfand, D.J. The FIRST Survey: Faint Images of the Radio Sky at Twenty Centimeters. *ApJ* **1995**, *450*, 559. doi:10.1086/176166.
14. Jiang, L.; Fan, X.; Bian, F.; McGreer, I.D.; Strauss, M.A.; Annis, J.; Buck, Z.; Green, R.; Hodge, J.A.; Myers, A.D.; Rafiee, A.; Richards, G. The Sloan Digital Sky Survey Stripe 82 Imaging Data: Depth-optimized Co-adds over 300 deg^2 in Five Filters. *ApJS* **2014**, *213*, 12, [arXiv:astro-ph.GA/1405.7382]. doi:10.1088/0067-0049/213/1/12.
15. Hodge, J.A.; Becker, R.H.; White, R.L.; Richards, G.T.; Zeimann, G.R. High-resolution Very Large Array Imaging of Sloan Digital Sky Survey Stripe 82 at 1.4 GHz. *AJ* **2011**, *142*, 3, [arXiv:astro-ph.CO/1103.5749]. doi:10.1088/0004-6256/142/1/3.
16. Smolčić, V.; Novak, M.; Bondi, M.; Ciliegi, P.; Mooley, K.P.; Schinnerer, E.; Zamorani, G.; Navarrete, F.; Bourke, S.; Karim, A.; Vardoulaki, E.; Leslie, S.; Delhaize, J.; Carilli, C.L.; Myers, S.T.; Baran, N.; Delvecchio, I.; Miettinen, O.; Banfield, J.; Baloković, M.; Bertoldi, F.; Capak, P.; Frail, D.A.; Hallinan, G.; Hao, H.; Herrera Ruiz, N.; Horesh, A.; Ilbert, O.; Intema, H.; Jelić, V.; Klöckner, H.R.; Krpan, J.; Kulkarni, S.R.; McCracken, H.; Laigle, C.; Middleberg, E.; Murphy, E.J.; Sargent, M.; Scoville, N.Z.; Sheth, K. The VLA-COSMOS 3 GHz Large Project: Continuum data and source catalog release. *A&A* **2017**, *602*, A1, [arXiv:astro-ph.GA/1703.09713]. doi:10.1051/0004-6361/201628704.
17. Schinnerer, E.; Smolčić, V.; Carilli, C.L.; Bondi, M.; Ciliegi, P.; Jahnke, K.; Scoville, N.Z.; Aussel, H.; Bertoldi, F.; Blain, A.W.; Impey, C.D.; Koekemoer, A.M.; Le Fevre, O.; Urry, C.M. The VLA-COSMOS Survey. II. Source Catalog of the Large Project. *ApJS* **2007**, *172*, 46–69, [astro-ph/0612314]. doi:10.1086/516587.
18. Shimwell, T. W..; Röttgering, H. J. A..; Best, P. N..; Williams, W. L..; Dijkema, T. J..; de Gasperin, F..; Hardcastle, M. J..; Heald, G. H..; Hoang, D. N..; Horneffer, A..; Intema, H..; Mahony, E. K..; Mandal, S..; Mechev, A. P..; Morabito, L..; Oonk, J. B. R..; Rafferty, D..; Retana-Montenegro, E..; Sabater, J..; Tasse, C..; van Weeren, R. J..; Brüggen, M..; Brunetti, G..; Chyzy, K. T..; Conway, J. E..; Haverkorn, M..; Jackson, N..; Jarvis, M. J..; McKean, J. P..; Miley, G. K..; Morganti, R..; White, G. J..; Wise, M. W..; van Bemmel, I. M..; Beck, R..; Brienza, M..; Bonafede, A..; Calistro Rivera, G..; Cassano, R..; Clarke, A. O..; Cseh, D..; Deller, A..; Drabent, A..; van Driel, W..; Engels, D..; Falcke, H..; Ferrari, C..; Fröhlich, S..; Garrett, M. A..; Harwood, J. J..; Heesen, V..; Hoeft, M..; Horellou, C..; Israel, F. P..; Kapi´nska, A. D..; Kunert-Bajraszewska, M..; McKay, D. J..; Mohan, N. R..; Orrú, E..; Pizzo, R. F..; Prandoni, I..;

Schwarz, D. J..; Shulevski, A..; Sipior, M..; Smith, D. J. B..; Sridhar, S. S..; Steinmetz, M..; Stroe, A..; Varenius, E..; van der Werf, P. P..; Zensus, J. A..; Zwart, J. T. L.. The LOFAR Two-metre Sky Survey - I. Survey description and preliminary data release. *A&A* **2017**, *598*, A104. doi:10.1051/0004-6361/201629313.

19. Shimwell, T.W.; Tasse, C.; Hardcastle, M.J.; Mechev, A.P.; Williams, W.L.; Best, P.N.; Röttgering, H.J.A.; Callingham, J.R.; Dijkema, T.J.; de Gasperin, F.; Hoang, D.N.; Hugo, B.; Mirmont, M.; Oonk, J.B.R.; Prandoni, I.; Rafferty, D.; Sabater, J.; Smirnov, O.; van Weeren, R.J.; White, G.J.; Atemkeng, M.; Bester, L.; Bonnassieux, E.; Brüggen, M.; Brunetti, G.; Chyży, K.T.; Cochrane, R.; Conway, J.E.; Croston, J.H.; Danezi, A.; Duncan, K.; Haverkorn, M.; Heald, G.H.; Iacobelli, M.; Intema, H.T.; Jackson, N.; Jamrozy, M.; Jarvis, M.J.; Lakhoo, R.; Mevius, M.; Miley, G.K.; Morabito, L.; Morganti, R.; Nisbet, D.; Orrú, E.; Perkins, S.; Pizzo, R.F.; Schrijvers, C.; Smith, D.J.B.; Vermeulen, R.; Wise, M.W.; Alegre, L.; Bacon, D.J.; van Bemmel, I.M.; Beswick, R.J.; Bonafede, A.; Botteon, A.; Bourke, S.; Brienza, M.; Calistro Rivera, G.; Cassano, R.; Clarke, A.O.; Conselice, C.J.; Dettmar, R.J.; Drabent, A.; Dumba, C.; Emig, K.L.; Enßlin, T.A.; Ferrari, C.; Garrett, M.A.; Génova-Santos, R.T.; Goyal, A.; Gürkan, G.; Hale, C.; Harwood, J.J.; Heesen, V.; Hoeft, M.; Horellou, C.; Jackson, C.; Kokotanekov, G.; Kondapally, R.; Kunert-Bajraszewska, M.; Mahatma, V.; Mahony, E.K.; Mandal, S.; McKean, J.P.; Merloni, A.; Mingo, B.; Miskolczi, A.; Mooney, S.; Nikiel-Wroczyński, B.; O'Sullivan, S.P.; Quinn, J.; Reich, W.; Roskowiński, C.; Rowlinson, A.; Savini, F.; Saxena, A.; Schwarz, D.J.; Shulevski, A.; Sridhar, S.S.; Stacey, H.R.; Urquhart, S.; van der Wiel, M.H.D.; Varenius, E.; Webster, B.; Wilber, A. The LOFAR Two-metre Sky Survey. II. First data release. *A&A* **2019**, *622*, A1, [arXiv:astro-ph.GA/1811.07926]. doi:10.1051/0004-6361/201833559.
20. Pâris, I.; Petitjean, P.; Aubourg, É.; Myers, A.D.; Streblyanska, A.; Lyke, B.W.; Anderson, S.F.; Armengaud, É.; Bautista, J.; Blanton, M.R.; Blomqvist, M.; Brinkmann, J.; Brownstein, J.R.; Brand t, W.N.; Burtin, É.; Dawson, K.; de la Torre, S.; Georgakakis, A.; Gil-Marín, H.; Green, P.J.; Hall, P.B.; Kneib, J.P.; LaMassa, S.M.; Le Goff, J.M.; MacLeod, C.; Mariappan, V.; McGreer, I.D.; Merloni, A.; Noterdaeme, P.; Palanque-Delabrouille, N.; Percival, W.J.; Ross, A.J.; Rossi, G.; Schneider, D.P.; Seo, H.J.; Tojeiro, R.; Weaver, B.A.; Weijmans, A.M.; Yèche, C.; Zarrouk, P.; Zhao, G.B. The Sloan Digital Sky Survey Quasar Catalog: Fourteenth data release. *A&A* **2018**, *613*, A51, [arXiv:astro-ph.GA/1712.05029]. doi:10.1051/0004-6361/201732445.
21. York, D.G.; Adelman, J.; Anderson, Jr., J.E.; Anderson, S.F.; Annis, J.; Bahcall, N.A.; Bakken, J.A.; Barkhouser, R.; Bastian, S.; Berman, E.; Boroski, W.N.; Bracker, S.; Briegel, C.; Briggs, J.W.; Brinkmann, J.; Brunner, R.; Burles, S.; Carey, L.; Carr, M.A.; Castander, F.J.; Chen, B.; Colestock, P.L.; Connolly, A.J.; Crocker, J.H.; Csabai, I.; Czarapata, P.C.; Davis, J.E.; Doi, M.; Dombeck, T.; Eisenstein, D.; Ellman, N.; Elms, B.R.; Evans, M.L.; Fan, X.; Federwitz, G.R.; Fiscelli, L.; Friedman, S.; Frieman, J.A.; Fukugita, M.; Gillespie, B.; Gunn, J.E.; Gurbani, V.K.; de Haas, E.; Haldeman, M.; Harris, F.H.; Hayes, J.; Heckman, T.M.; Hennessy, G.S.; Hindsley, R.B.; Holm, S.; Holmgren, D.J.; Huang, C.h.; Hull, C.; Husby, D.; Ichikawa, S.I.; Ichikawa, T.; Ivezić, Ž.; Kent, S.; Kim, R.S.J.; Kinney, E.; Klaene, M.; Kleinman, A.N.; Kleinman, S.; Knapp, G.R.; Korienek, J.; Kron, R.G.; Kunszt, P.Z.; Lamb, D.Q.; Lee, B.; Leger, R.F.; Limmongkol, S.; Lindenmeyer, C.; Long, D.C.; Loomis, C.; Loveday, J.; Lucinio, R.; Lupton, R.H.; MacKinnon, B.; Mannery, E.J.; Mantsch, P.M.; Margon, B.; McGehee, P.; McKay, T.A.; Meiksin, A.; Merelli, A.; Monet, D.G.; Munn, J.A.; Narayanan, V.K.; Nash, T.; Neilsen, E.; Neswold, R.; Newberg, H.J.; Nichol, R.C.; Nicinski, T.; Nonino, M.; Okada, N.; Okamura, S.; Ostriker, J.P.; Owen, R.; Pauls, A.G.; Peoples, J.; Peterson, R.L.; Petravick, D.; Pier, J.R.; Pope, A.; Pordes, R.; Prosapio, A.; Rechenmacher, R.; Quinn, T.R.; Richards, G.T.; Richmond, M.W.; Rivetta, C.H.; Rockosi, C.M.; Ruthmansdorfer, K.; Sandford, D.; Schlegel, D.J.; Schneider, D.P.; Sekiguchi, M.; Sergey, G.; Shimasaku, K.; Siegmund, W.A.; Smee, S.; Smith, J.A.; Snedden, S.; Stone, R.; Stoughton, C.; Strauss, M.A.; Stubbs, C.; SubbaRao, M.; Szalay, A.S.; Szapudi, I.; Szokoly, G.P.; Thakar, A.R.; Tremonti, C.; Tucker, D.L.; Uomoto, A.; Vanden Berk, D.; Vogeley, M.S.; Waddell, P.; Wang, S.i.; Watanabe, M.; Weinberg, D.H.; Yanny, B.; Yasuda, N.; SDSS Collaboration. The Sloan Digital Sky Survey: Technical Summary. *AJ* **2000**, *120*, 1579–1587, [astro-ph/0006396]. doi:10.1086/301513.
22. Dawson, K.S.; Schlegel, D.J.; Ahn, C.P.; Anderson, S.F.; Aubourg, É.; Bailey, S.; Barkhouser, R.H.; Bautista, J.E.; Beifiori, A.; Berlind, A.A.; Bhardwaj, V.; Bizyaev, D.; Blake, C.H.; Blanton, M.R.; Blomqvist, M.; Bolton, A.S.; Borde, A.; Bovy, J.; Brandt, W.N.; Brewington, H.; Brinkmann, J.; Brown, P.J.; Brownstein, J.R.; Bundy, K.; Busca, N.G.; Carithers, W.; Carnero, A.R.; Carr, M.A.; Chen, Y.; Comparat, J.; Connolly, N.; Cope, F.; Croft, R.A.C.; Cuesta, A.J.; da Costa, L.N.; Davenport, J.R.A.; Delubac, T.; de Putter, R.; Dhital, S.; Ealet, A.; Ebelke, G.L.; Eisenstein, D.J.; Escoffier, S.; Fan, X.; Filiz Ak, N.; Finley, H.; Font-Ribera, A.; Génova-Santos, R.; Gunn, J.E.; Guo, H.; Haggard, D.; Hall, P.B.; Hamilton, J.C.; Harris, B.; Harris, D.W.; Ho, S.; Hogg, D.W.; Holder, D.; Honscheid, K.; Huehnerhoff, J.; Jordan, B.; Jordan, W.P.; Kauffmann, G.; Kazin, E.A.; Kirkby, D.; Klaene, M.A.; Kneib, J.P.; Le Goff, J.M.; Lee, K.G.; Long, D.C.; Loomis, C.P.; Lundgren, B.; Lupton, R.H.; Maia, M.A.G.; Makler, M.; Malanushenko, E.; Malanushenko, V.; Mandelbaum, R.; Manera, M.; Maraston, C.; Margala, D.; Masters, K.L.; McBride, C.K.; McDonald, P.; McGreer, I.D.; McMahon, R.G.; Mena, O.; Miralda-Escudé, J.; Montero-Dorta, A.D.; Montesano, F.; Muna, D.; Myers, A.D.; Naugle, T.; Nichol, R.C.; Noterdaeme, P.; Nuza, S.E.; Olmstead, M.D.; Oravetz, A.; Oravetz, D.J.; Owen, R.; Padmanabhan, N.; Palanque-Delabrouille, N.; Pan, K.; Parejko, J.K.; Pâris, I.; Percival, W.J.; Pérez-Fournon, I.; Pérez-Ràfols, I.; Petitjean, P.; Pfaffenberger, R.; Pforr, J.; Pieri, M.M.; Prada, F.; Price-Whelan, A.M.; Raddick, M.J.; Rebolo, R.; Rich, J.; Richards, G.T.; Rockosi, C.M.; Roe, N.A.; Ross, A.J.; Ross, N.P.; Rossi, G.; Rubiño-Martin, J.A.; Samushia, L.; Sánchez, A.G.; Sayres, C.; Schmidt, S.J.; Schneider, D.P.; Scóccola, C.G.; Seo, H.J.; Shelden, A.; Sheldon, E.; Shen, Y.; Shu, Y.; Slosar, A.; Smee, S.A.; Snedden, S.A.; Stauffer, F.; Steele, O.; Strauss, M.A.; Streblyanska, A.; Suzuki, N.; Swanson, M.E.C.; Tal, T.; Tanaka, M.; Thomas, D.; Tinker, J.L.; Tojeiro, R.; Tremonti, C.A.; Vargas Magaña, M.; Verde, L.; Viel, M.; Wake, D.A.; Watson, M.; Weaver, B.A.; Weinberg, D.H.; Weiner, B.J.; West, A.A.; White, M.; Wood-Vasey, W.M.; Yeche, C.; Zehavi, I.; Zhao, G.B.; Zheng, Z. The Baryon Oscillation Spectroscopic Survey of SDSS-III. *AJ* **2013**, *145*, 10, [1208.0022]. doi:10.1088/0004-6256/145/1/10.

23. Eisenstein, D.J.; Weinberg, D.H.; Agol, E.; Aihara, H.; Allende Prieto, C.; Anderson, S.F.; Arns, J.A.; Aubourg, É.; Bailey, S.; Balbinot, E.; et al.. SDSS-III: Massive Spectroscopic Surveys of the Distant Universe, the Milky Way, and Extra-Solar Planetary Systems. *AJ* **2011**, *142*, 72, [arXiv:astro-ph.IM/1101.1529]. doi:10.1088/0004-6256/142/3/72.
24. Dawson, K.S.; Kneib, J.P.; Percival, W.J.; Alam, S.; Albareti, F.D.; Anderson, S.F.; Armengaud, E.; Aubourg, É.; Bailey, S.; Bautista, J.E.; Berlind, A.A.; Bershady, M.A.; Beutler, F.; Bizyaev, D.; Blanton, M.R.; Blomqvist, M.; Bolton, A.S.; Bovy, J.; Brandt, W.N.; Brinkmann, J.; Brownstein, J.R.; Burtin, E.; Busca, N.G.; Cai, Z.; Chuang, C.H.; Clerc, N.; Comparat, J.; Cope, F.; Croft, R.A.C.; Cruz-Gonzalez, I.; da Costa, L.N.; Cousinou, M.C.; Darling, J.; de la Macorra, A.; de la Torre, S.; Delubac, T.; du Mas des Bourboux, H.; Dwelly, T.; Ealet, A.; Eisenstein, D.J.; Eracleous, M.; Escoffier, S.; Fan, X.; Finoguenov, A.; Font-Ribera, A.; Frinchaboy, P.; Gaulme, P.; Georgakakis, A.; Green, P.; Guo, H.; Guy, J.; Ho, S.; Holder, D.; Huehnerhoff, J.; Hutchinson, T.; Jing, Y.; Jullo, E.; Kamble, V.; Kinemuchi, K.; Kirkby, D.; Kitaura, F.S.; Klaene, M.A.; Laher, R.R.; Lang, D.; Laurent, P.; Le Goff, J.M.; Li, C.; Liang, Y.; Lima, M.; Lin, Q.; Lin, W.; Lin, Y.T.; Long, D.C.; Lundgren, B.; MacDonald, N.; Geimba Maia, M.A.; Malanushenko, E.; Malanushenko, V.; Mariappan, V.; McBride, C.K.; McGreer, I.D.; Ménard, B.; Merloni, A.; Meza, A.; Montero-Dorta, A.D.; Muna, D.; Myers, A.D.; Nandra, K.; Naugle, T.; Newman, J.A.; Noterdaeme, P.; Nugent, P.; Ogando, R.; Olmstead, M.D.; Oravetz, A.; Oravetz, D.J.; Padmanabhan, N.; Palanque-Delabrouille, N.; Pan, K.; Parejko, J.K.; Pâris, I.; Peacock, J.A.; Petitjean, P.; Pieri, M.M.; Pisani, A.; Prada, F.; Prakash, A.; Raichoor, A.; Reid, B.; Rich, J.; Ridl, J.; Rodriguez-Torres, S.; Carnero Rosell, A.; Ross, A.J.; Rossi, G.; Ruan, J.; Salvato, M.; Sayres, C.; Schneider, D.P.; Schlegel, D.J.; Seljak, U.; Seo, H.J.; Sesar, B.; Shandera, S.; Shu, Y.; Slosar, A.; Sobreira, F.; Streblyanska, A.; Suzuki, N.; Taylor, D.; Tao, C.; Tinker, J.L.; Tojeiro, R.; Vargas-Magaña, M.; Wang, Y.; Weaver, B.A.; Weinberg, D.H.; White, M.; Wood-Vasey, W.M.; Yeche, C.; Zhai, Z.; Zhao, C.; Zhao, G.b.; Zheng, Z.; Ben Zhu, G.; Zou, H. The SDSS-IV Extended Baryon Oscillation Spectroscopic Survey: Overview and Early Data. *AJ* **2016**, *151*, 44, [arXiv:astro-ph.CO/1508.04473]. doi:10.3847/0004-6256/151/2/44.
25. Stern, D.; Eisenhardt, P.; Gorjian, V.; Kochanek, C.S.; Caldwell, N.; Eisenstein, D.; Brodwin, M.; Brown, M.J.I.; Cool, R.; Dey, A.; Green, P.; Jannuzi, B.T.; Murray, S.S.; Pahre, M.A.; Willner, S.P. Mid-Infrared Selection of Active Galaxies. *ApJ* **2005**, *631*, 163–168, [arXiv:astro-ph/astro-ph/0410523]. doi:10.1086/432523.
26. Lacy, M.; Canalizo, G.; Rawlings, S.; Sajina, A.; Storrie-Lombardi, L.; Armus, L.; Marleau, F.R.; Muzzin, A. Mid-infrared selection of Quasar-2s in Spitzer's First Look Survey. *Mem. Soc. Astron. Italian* **2005**, *76*, 154, [arXiv:astro-ph/astro-ph/0411416].
27. Stern, D.; Assef, R.J.; Benford, D.J.; Blain, A.; Cutri, R.; Dey, A.; Eisenhardt, P.; Griffith, R.L.; Jarrett, T.H.; Lake, S.; Masci, F.; Petty, S.; Stanford, S.A.; Tsai, C.W.; Wright, E.L.; Yan, L.; Harrison, F.; Madsen, K. Mid-infrared Selection of Active Galactic Nuclei with the Wide-Field Infrared Survey Explorer. I. Characterizing WISE-selected Active Galactic Nuclei in COSMOS. *ApJ* **2012**, *753*, 30, [arXiv:astro-ph.CO/1205.0811]. doi:10.1088/0004-637X/753/1/30.
28. Assef, R.J.; Stern, D.; Kochanek, C.S.; Blain, A.W.; Brodwin, M.; Brown, M.J.I.; Donoso, E.; Eisenhardt, P.R.M.; Jannuzi, B.T.; Jarrett, T.H.; Stanford, S.A.; Tsai, C.W.; Wu, J.; Yan, L. Mid-infrared Selection of Active Galactic Nuclei with the Wide-field Infrared Survey Explorer. II. Properties of WISE-selected Active Galactic Nuclei in the NDWFS Boötes Field. *ApJ* **2013**, *772*, 26, [arXiv:astro-ph.CO/1209.6055]. doi:10.1088/0004-637X/772/1/26.
29. Wright, E.L.; Eisenhardt, P.R.M.; Mainzer, A.K.; Ressler, M.E.; Cutri, R.M.; Jarrett, T.; Kirkpatrick, J.D.; Padgett, D.; McMillan, R.S.; Skrutskie, M.; Stanford, S.A.; Cohen, M.; Walker, R.G.; Mather, J.C.; Leisawitz, D.; Gautier, III, T.N.; McLean, I.; Benford, D.; Lonsdale, C.J.; Blain, A.; Mendez, B.; Irace, W.R.; Duval, V.; Liu, F.; Royer, D.; Heinrichsen, I.; Howard, J.; Shannon, M.; Kendall, M.; Walsh, A.L.; Larsen, M.; Cardon, J.G.; Schick, S.; Schwalm, M.; Abid, M.; Fabinsky, B.; Naes, L.; Tsai, C.W. The Wide-field Infrared Survey Explorer (WISE): Mission Description and Initial On-orbit Performance. *AJ* **2010**, *140*, 1868–1881, [arXiv:astro-ph.IM/1008.0031]. doi:10.1088/0004-6256/140/6/1868.
30. Lake, S.E.; Wright, E.L.; Petty, S.; Assef, R.J.; Jarrett, T.H.; Stanford, S.A.; Stern, D.; Tsai, C.W. OPTICAL SPECTROSCOPIC SURVEY OF HIGH-LATITUDEWISE-SELECTED SOURCES. *AJ* **2011**, *143*, 7. doi:10.1088/0004-6256/143/1/7.
31. Cameron, E. On the Estimation of Confidence Intervals for Binomial Population Proportions in Astronomy: The Simplicity and Superiority of the Bayesian Approach. *PASA* **2011**, *28*, 128–139, [arXiv:astro-ph.IM/1012.0566]. doi:10.1071/AS10046.
32. Stanley, F.; Harrison, C.M.; Alexander, D.M.; Swinbank, A.M.; Aird, J.A.; Del Moro, A.; Hickox, R.C.; Mullaney, J.R. A remarkably flat relationship between the average star formation rate and AGN luminosity for distant X-ray AGN. *MNRAS* **2015**, *453*, 591–604, [http://oup.prod.sis.lan/mnras/article-pdf/453/1/591/4935266/stv1678.pdf]. doi:10.1093/mnras/stv1678.
33. Smolčić.; Delvecchio, I..; Zamorani, G..; Baran, N..; Novak, M..; Delhaize, J..; Schinnerer, E..; Berta, S..; Bondi, M..; Ciliegi, P..; Capak, P..; Civano, F..; Karim, A..; Le Fevre, O..; Ilbert, O..; Laigle, C..; Marchesi, S..; McCracken, H. J..; Tasca, L..; Salvato, M..; Vardoulaki, E.. The VLA-COSMOS 3 GHz Large Project: Multiwavelength counterparts and the composition of the faint radio population. *A&A* **2017**, *602*, A2. doi:10.1051/0004-6361/201630223.
34. Intema, H.T.; Jagannathan, P.; Mooley, K.P.; Frail, D.A. The GMRT 150 MHz all-sky radio survey. First alternative data release TGSS ADR1. *A&A* **2017**, *598*, A78, [arXiv:astro-ph.CO/1603.04368]. doi:10.1051/0004-6361/201628536.
35. Orienti, M.; Dallacasa, D. Physical properties of young radio sources: VLBA observations of high-frequency peaking radio sources. *MNRAS* **2013**, *438*, 463–475, [https://academic.oup.com/mnras/article-pdf/438/1/463/18463416/stt2217.pdf]. doi:10.1093/mnras/stt2217.
36. Vernet, J.; Dekker, H.; D'Odorico, S.; Kaper, L.; Kjaergaard, P.; Hammer, F.; Randich, S.; Zerbi, F.; Groot, P.J.; Hjorth, J.; Guinouard, I.; Navarro, R.; Adolfse, T.; Albers, P.W.; Amans, J.P.; Andersen, J.J.; Andersen, M.I.; Binetruy, P.; Bristow, P.; Castillo, R.; Chemla, F.; Christensen, L.; Conconi, P.; Conzelmann, R.; Dam, J.; de Caprio, V.; de Ugarte Postigo, A.; Delabre, B.; di Marcantonio, P.; Downing, M.; Elswijk, E.; Finger, G.; Fischer, G.; Flores, H.; François, P.; Goldoni, P.; Guglielmi, L.; Haigron, R.; Hanenburg,

H.; Hendriks, I.; Horrobin, M.; Horville, D.; Jessen, N.C.; Kerber, F.; Kern, L.; Kiekebusch, M.; Kleszcz, P.; Klougart, J.; Kragt, J.; Larsen, H.H.; Lizon, J.L.; Lucuix, C.; Mainieri, V.; Manuputy, R.; Martayan, C.; Mason, E.; Mazzoleni, R.; Michaelsen, N.; Modigliani, A.; Moehler, S.; Møller, P.; Norup Sørensen, A.; Nørregaard, P.; Péroux, C.; Patat, F.; Pena, E.; Pragt, J.; Reinero, C.; Rigal, F.; Riva, M.; Roelfsema, R.; Royer, F.; Sacco, G.; Santin, P.; Schoenmaker, T.; Spano, P.; Sweers, E.; Ter Horst, R.; Tintori, M.; Tromp, N.; van Dael, P.; van der Vliet, H.; Venema, L.; Vidali, M.; Vinther, J.; Vola, P.; Winters, R.; Wistisen, D.; Wulterkens, G.; Zacchei, A. X-shooter, the new wide band intermediate resolution spectrograph at the ESO Very Large Telescope. *A&A* **2011**, *536*, A105, [arXiv:astro-ph.IM/1110.1944]. doi:10.1051/0004-6361/201117752.

37. Trump, J.R.; Hall, P.B.; Reichard, T.A.; Richards, G.T.; Schneider, D.P.; Vanden Berk, D.E.; Knapp, G.R.; Anderson, S.F.; Fan, X.; Brinkman, J.; Kleinman, S.J.; Nitta, A. A Catalog of Broad Absorption Line Quasars from the Sloan Digital Sky Survey Third Data Release. *ApJS* **2006**, *165*, 1–18, [arXiv:astro-ph/astro-ph/0603070]. doi:10.1086/503834.
38. Morabito, L.K.; Matthews, J.H.; Best, P.N.; Gürkan, G.; Jarvis, M.J.; Prandoni, I.; Duncan, K.J.; Hardcastle, M.J.; Kunert-Bajraszewska, M.; Mechev, A.P.; Mooney, S.; Sabater, J.; Röttgering, H.J.A.; Shimwell, T.W.; Smith, D.J.B.; Tasse, C.; Williams, W.L. The origin of radio emission in broad absorption line quasars: Results from the LOFAR Two-metre Sky Survey. *A&A* **2019**, *622*, A15, [arXiv:astro-ph.GA/1811.07931]. doi:10.1051/0004-6361/201833821.
39. Martini, P.; Bailey, S.; Besuner, R.W.; Brooks, D.; Doel, P.; Edelstein, J.; Eisenstein, D.; Flaugher, B.; Gutierrez, G.; Harris, S.E.; Honscheid, K.; Jelinsky, P.; Joyce, R.; Kent, S.; Levi, M.; Prada, F.; Poppett, C.; Rabinowitz, D.; Rockosi, C.; Cardiel Sas, L.; Schlegel, D.J.; Schubnell, M.; Sharples, R.; Silber, J.H.; Sprayberry, D.; Wechsler, R. Overview of the Dark Energy Spectroscopic Instrument. Ground-based and Airborne Instrumentation for Astronomy VII; Evans, C.J.; Simard, L.; Takami, H., Eds., 2018, Vol. 10702, *Society of Photo-Optical Instrumentation Engineers (SPIE) Conference Series*, p. 107021F, [arXiv:astro-ph.IM/1807.09287]. doi:10.1117/12.2313063.